An Autoregressive Model-Based Particle Filtering Algorithms for Extraction of Respiratory Rates as High as 90 Breaths Per Minute From Pulse Oximeter

Jinseok Lee*, *Member, IEEE*, and Ki H. Chon, *Senior Member, IEEE*

***Abstract*—We present particle filtering (PF) algorithms for an accurate respiratory rate extraction from pulse oximeter recordings over a broad range: 12–90 breaths/min. These methods are based on an autoregressive (AR) model, where the aim is to find the pole angle with the highest magnitude as it corresponds to the respiratory rate. However, when SNR is low, the pole angle with the highest magnitude may not always lead to accurate estimation of the respiratory rate. To circumvent this limitation, we propose a probabilistic approach, using a sequential Monte Carlo method, named PF, which is combined with the optimal parameter search (OPS) criterion for an accurate AR model-based respiratory rate extraction. The PF technique has been widely adopted in many tracking applications, especially for nonlinear and/or non-Gaussian problems. We examine the performances of five different likelihood functions of the PF algorithm: the strongest neighbor, nearest neighbor (NN), weighted nearest neighbor (WNN), probability data association (PDA), and weighted probability data association (WPDA). The performance of these five combined OPS-PF algorithms was measured against a solely OPS-based AR algorithm for respiratory rate extraction from pulse oximeter recordings. The pulse oximeter data were collected from 33 healthy subjects with breathing rates ranging from 12 to 90 breaths/ min. It was found that significant improvement in accuracy can be achieved by employing particle filters, and that the combined OPS-PF employing either the NN or WNN likelihood function achieved the best results for all respiratory rates considered in this paper. The main advantage of the combined OPS-PF with either the NN or WNN likelihood function is that for the first time, respiratory rates as high as 90 breaths/min can be accurately extracted from pulse oximeter recordings.**

***Index Terms*—Autoregressive (AR) model, optimal parameter search (OPS), particle filter, pulse oximeters, respiratory rate extraction.**

I. Introduction

RESPIRATORY rate is one of the important vital signs, and much effort has been centered on extracting it from pulse oximeter and electrocardiogram recordings [1]–[4]. The research has been driven largely by the desire to reduce the number of sensors that need to be connected to a patient to obtain vital signs.

Recent promising approaches based on time-frequency spectral techniques have been used to extract respiratory rates directly from a pulse oximeter [1]–[3], [5]–[8]. With recognition that respiration modulates heart rate and that they are both time-varying, time-frequency analyses were used to extract the former signal. Specifically, the continuous wavelet transform (CWT) [5], [6] and variable frequency complex demodulation (VFCDM) [1], [8] methods were utilized to extract either frequency modulation or amplitude modulation seen in the frequency range associated to the heart rate. Both CWT and VFCDM methods have been shown to provide accurate respiratory rate extraction in the low- and moderate-breathing rates (12–36 breaths/min). However, these time-frequency methods' capability became less reliable with increased respiratory rates [1].

Recently, an autoregressive (AR) model method, utilizing the optimal parameter search (OPS) technique [9], [10] showed accurate respiratory rate extraction especially for high-breathing rates (36–48 breaths/min) [11]. The AR method involves factorizing the estimated AR parameters into multiple pole terms. The pole with the highest magnitude is chosen to represent a respiratory rate. The accuracy of our technique using an AR model should be aided by the OPS as it has been shown to be more accurate than the well-known model order criteria such as Akaike information criterion, minimum description length, and the fast orthogonal search criterion [10], [12]–[15]. However, as the SNR decreases, the probability increases that incorrect poles are associated with the highest magnitude, which ultimately affects the accuracy of the method.

To mitigate the previously described limitation of the AR model, we used a sequential Monte Carlo method, known as particle filtering (PF) [16], [17]. The PF method has gained much recognition in recent years and has mainly been used for tracking moving targets [18], [19]. Recently, much effort has centered on developing efficient PF algorithms for real-time implementation [20], [21].

In this paper, we formulate a general framework for respiratory extraction based on the PF algorithm combined with OPS. Specifically, we examine five different likelihood functions for estimating the probability density function. These five different likelihood functions were examined to determine which among the five provided the best results for varying levels of SNR and breathing rates. The efficacy of our proposed PF-OPS algorithm

Manuscript received March 15, 2010; revised May 12, 2010; accepted May 18, 2010. Date of publication June 10, 2010; date of current version August 18, 2010. This work was supported in part by the Office of Naval Research work unit N00014-08-1-0244. *Asterisk indicates corresponding author.*

*J. Lee is with the Department of Biomedical Engineering, Worcester Polytechnic Institute, Worcester, MA 01609 USA (e-mail: jinseok@wpi.edu).

K. H. Chon is with the Department of Biomedical Engineering, Worcester Polytechnic Institute, Worcester, MA 01609 USA (e-mail: kichon@wpi.edu).

Color versions of one or more of the figures in this paper are available online at http://ieeexplore.ieee.org.

Digital Object Identifier 10.1109/TBME.2010.2051330

was examined by comparing it to the OPS-based AR model without PF, using pulse oximeter recordings from 33 healthy human subjects breathing at 12, 18, 24, 30, 36, 42, 48, 60, 72, and 90 breaths/ min.

II. Method

A. Respiratory Rate Extraction With AR Model

Our approach to extract respiratory rates from photoplethysmograph (PPG) is to use combined OPS-PF algorithms. Respiratory rates are formulated as an AR model

$$x(n) = -\sum_{k=1}^{K} a_k x(n-k) + e(n) \tag{1}$$

where K is the model order, a_k are the unknown coefficients, and $e(n)$ is the prediction error. We use the OPS to obtain accurate parameter estimation among the overdetermined model order K. The OPS can be designed to automatically select the optimal model order for any signal, thus, can be tuned to each signal without any human subjectivity. With any initial model order of K, the significant model order K_{opt} is determined by the ratio of two neighboring projection distances [13]. Once the unknown AR parameters a_k are estimated, they are formulated as the transfer function $H(z)$ as follows:

$$H(z) = \frac{1}{\sum_{k=1}^{K_{\text{ops}}} a_k z^{-k}} = \frac{z^{K_{\text{ops}}}}{(z-z_1)(z-z_2)\dots(z-z_{K_{\text{ops}}})} \tag{2}$$

where the AR coefficients are factorized into K_{ops} pole terms, where $K_{\text{ops}} \leq K$. The real and complex conjugate poles define the power spectral peaks with the larger magnitude poles corresponding to the greater magnitudes [11], [22]. The resonant frequency of each spectral peak is given by the phase angle of the corresponding pole; the phase angle θ of a pole at frequency f is defined as $2\pi f \Delta t$, where Δt is the sampling interval. Among the poles, we set the region of interest (ROI) for respiratory rates between f_{low} and f_{high} (e.g., 0.15 and 1.5 Hz). Let us denote the number of the pole angles within the ROI by K_{roi}. If $K_{\text{roi}} \geq 2$, the pole with the highest magnitude is chosen to be representative of the respiratory rate.

In previous studies, the OPS showed better performance than both CWT [2], [3], [5]–[7], [23] and VFCDM [1], [8]-based time-frequency spectral techniques for high respiratory rates (higher than 0.6 Hz) but not at lower breathing rates (0.2–0.6 Hz). The main advantage of the OPS was found to be that the computational speed was approximately five times faster than VFCDM and 30 times faster than CWT. In addition, the OPS, because it is an AR-model-based method, can perform reliable respiratory rate estimation using only half of the data required by either the CWT or VFCDM methods.

The aim of the study was to improve the accuracy of an AR model approach compared to the time-frequency methods for lower breathing rates and to extend capability to extract respiratory rates as high as 90 breaths/min. To illustrate the limitation of the OPS-model-based respiratory rate extraction, a simple simulation example is provided to show how and when the method succumbs to noise perturbation. The test signal involves two frequencies chosen so that they represent the frequency responses of the heart rate and the normal respiratory rate, as shown shortly [11]:

TABLE I
False Detection of 0.6070 With −10 dB SNR: Angles and Magnitudes of Candidate Poles at Time 60 S in Fig. 1(b)

Angle	**0.6070**	0.6066	0.4022	**0.3997**	0.2403
Magnitude	**0.9887**	0.1929	0.8003	**0.9852**	0.9433

$$y(n) = A_h \cos\left(2\pi f_h(n)\frac{n}{f_s} + \phi_h\right) + A_b \cos\left(2\pi f_b(n)\frac{n}{f_s} + \phi_b\right) + N_e \tag{3}$$

where $f_h(n)$ and $f_b(n)$ are the heart rate and respiratory rate, respectively. ϕ_h and ϕ_b are phases associated to the heart rate and respiratory rates, respectively, and f_s is the sampling rate. For the simulation example, A_h and A_b were set to 10 and 1, respectively. The $f_h(n)$ and $f_b(n)$ were set to 2.0 and 0.4 Hz, respectively, and ϕ_h and ϕ_b were randomly generated between 0 and 2π with uniform distribution. In addition, we corrupted the signal with two different levels of Gaussian white noise (GWN) N_e so that the SNR are -5 and -10 dB. We generated 60 000 samples for both SNR with a sampling rate of 100 Hz, which resulted in 10 min of data. We performed the respiratory rate estimation on 60-s segment waveforms of the test signal, and the waveform segment was shifted by 10-s for the entire 10-min duration. Thus, each 60-s segment waveform had a 50-s overlap, and 55 segments were obtained for the entire signal. To increase the angular resolution of the low frequency (LF) information and because we are only interested in respiratory rates up to 1.5 Hz, each windowed waveform was down sampled to 3 Hz. Using the OPS technique, we selected an AR model order of 20, and the calculated AR parameters were formulated as the transfer function of (2). Fig. 1 shows the estimation result based on the SNR of -5 and -10 dB for each of the 55 segments. Note that there is a lag in the results in Fig. 1 since our data analysis is based on 60 s segments. It is shown that as the SNR decreases, the probability that incorrect poles are associated with the highest magnitude increases. More specifically, we list the resultant pole angles and magnitudes at time 60 s for an SNR of -10 dB in Table I. The pole angle of 0.3997 Hz, which is closest to the true rate of 0.4 Hz, has the magnitude of 0.9852. On the other hand, the pole angle of 0.6070 Hz has the magnitude of 0.9887, and consequently, is chosen as the respiratory rate since it has the largest magnitude among all chosen poles. Thus, with this choice, we have an error of 0.2 Hz deviation from the true respiratory rate.

B. Development of a General Framework

We formulated a general framework for respiratory extraction based on PF combined with the OPS technique. Let us denote a true PPG waveform from time $n - n_{\text{seg}}$ to time n by $S_{n-n_{\text{seg}}:n}$ (e.g., n_{seg} represents a waveform segment). Based on the waveform of $S_{n-n_{\text{seg}}:n}$, we define the respiratory state at time n as $R(n)$. By using the OPS technique and the breathing

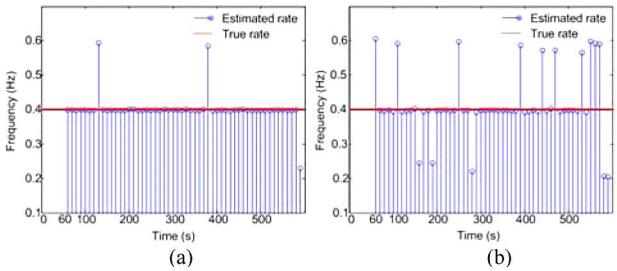

Fig. 1. Test signal is corrupted with additive Gaussian white noise (AGWN) for SNR (a) −5 dB and (b) −10 dB. Based on the OPS technique, the rates are estimated. As SNR decreases, the chance that false poles have the highest magnitude is increasing.

Form an initial set of particles, $R^i(0)$, $i=1,\ldots I$, and give them uniform weights $w^i(0) = 1/I$.

1. Predict the new set of particles $R^i(n)$ by propagating the resampled set $\bar{R}^i(n-n_{sam})$

2. Obtain measurement $\boldsymbol{P}(n)$ by the OPS model in the region of interest.

3. Evaluate each particle weight $w^i(n)$ according to likelihood functions $p(\boldsymbol{P}(n)|R^i(n))$

4. Compute the respiratory state (rate) $R(n)$ as the weighted sum of particles $E[R^i(n)]=\Sigma^I_{i=1} w^i(n)R^i(n)$

5. Resample the particles, $\bar{R}^i(n)$

Fig. 2. Generic PF algorithm for respiratory rate extraction.

rates' ROI, we obtain $K_{\rm roi}$ pairs of pole angles and their magnitudes. Let us denote the pairs of pole angles and magnitudes by the measurement vector $\boldsymbol{P}(n)$.

$$\boldsymbol{P}(n) = f_{\rm ops}\left(S_{n-n_{\rm seg}:n}, Q_1(n)\right) \tag{4}$$

where $f_{\rm ops}(\cdot)$ is a function of the OPS and the ROI, and $Q_1(n)$ is a noise term, which is not necessarily Gaussian. The measurement vector obtained by the OPS technique is represented by a $2K_{\rm roi}$-dimensional parameter vector with the first $K_{\rm roi}$ parameters representing $K_{\rm roi}$-pole angles, and the last $K_{\rm roi}$ parameters representing $K_{\rm roi}$-pole magnitudes.

$$\boldsymbol{P}(n) = \left[p_1^a\, p_2^a \cdots p_k^a \cdots p_{K_{\rm roi}}^a p_1^m\, p_2^m \cdots p_k^m \cdots p_{K_{\rm roi}}^m\right]^T \tag{5}$$

where p_k^a and p_k^m represent kth pole angle and magnitude, respectively.

We assume that the respiratory state is a Markov process, which can be modeled by the state transition relation as

$$R(n) = T\left(R(n-n_{\rm sam}), Q_2(n)\right) \tag{6}$$

where $T(\cdot)$ is a known, not necessarily linear function of the previous state at time sample $n-n_{\rm sam}$ and $Q_2(n)$ is a noise term, which is not necessarily Gaussian.

Let $\boldsymbol{P} = (1:n) = [\boldsymbol{P}(1)\ldots\boldsymbol{P}(n-n_{\rm sam})\ \boldsymbol{P}(n)]$ denotes the concatenation of all measurements up to time n. The aim is to recursively estimate the conditional probability density $p(R(n)\,|\boldsymbol{P}(1:n))$, from which the respiratory rate can be obtained as the mean of the density function. In practice, the posterior probability density is not available. However, assuming that the posterior probability density at time $n-n_{\rm sam}$ is available, the posterior probability density at time n can be found through the Chapman–Kolmogorov equation and Bayes' rule

$$\begin{aligned} &p(R(n)\,|\boldsymbol{P}(1:n-n_{\rm sam}))\\ &= \int p(R(n)\,|R(n-1))p(R(n-n_{\rm sam})\,|\boldsymbol{P}(1:n-n_{\rm sam}))\\ &\quad \times dR(n-n_{\rm sam}) \end{aligned} \tag{7}$$

$$p(R(n)|\boldsymbol{P}(1:n)) \propto p(\boldsymbol{P}(n)|R(n))p(R(n)|\boldsymbol{P}(1:n-n_{\rm sam})) \tag{8}$$

where $p(R(n)\,|\boldsymbol{P}(1:n-n_{\rm sam}))$ is the posterior probability density, $p(R(n)\,|R(n-n_{\rm sam}))$ is the state transition density, $p(R(n)\,|\boldsymbol{P}(1:n))$ is the prediction probability density, and $p(\boldsymbol{P}(n)\,|R(n))$ is the likelihood.

In general, no closed-form solution exists for (7) and (8) except in the special case, where $f_{\rm ops}(\cdot)$ and $T(\cdot)$ in (4) and (6) are linear functions, and the noises $Q_1(n)$ and $Q_2(n)$ are Gaussian. In this case, the Kalman filter is the optimal solution. However, the pole angles obtained from the OPS method as well as Burg's method were found to have a non-Gaussian distribution [1], [11]. Hence, we use a PF approach, which is suitable for non-Gaussian problems, and approximate (7) and (8) via Monte Carlo simulations involving a set of particles. It has been shown that as the number of particles becomes large, their particle weights tend to approach the true distribution of the signal. Details concerning the generic PF algorithm are described in [16]. With the framework outlined mentioned earlier, the algorithm that we propose for respiratory rate extraction using PF is described in Fig. 2.

C. Particle Generation

The first step to particle generation is to represent a prior probability density function $p(R(n)|\boldsymbol{P}(1:n-n_{\rm sam}))$ by a set of particles. Given the particles corresponding to the posterior probability density function of $p(R(n-n_{\rm sam})|\boldsymbol{P}(1:n-n_{\rm sam}))$ obtained at time $n-n_{\rm sam}$, new particles are generated at time n as

$$R^i(n) = F\left(\bar{R}^i(n-n_{\rm sam})\right) + Q_2(n) \tag{9}$$

where $R^i(n)$ are the ith generated particles, $i=\{1,2,\ldots,I\}$ for the number of particles I, and $Q_2(n)$ is a Gaussian noise with $N\left(0,\sigma^2_{\rm gen}\right)$. In addition, we assume that $R(n)$ is a stationary process denoted as

$$F\left(R(n-n_{\rm sam})\right) = R(n-n_{\rm sam}). \tag{10}$$

Note that $\bar{R}^i(n-n_{\rm sam})$ represents resampled particles obtained at time $n-n_{\rm sam}$, and the resampling process will be explained in the proceeding section.

D. Weight Evaluation With Proposed Likelihood Functions

After the new particles corresponding to the prior probability density function $p(R(n)\,|\boldsymbol{P}(1:n-n_{\rm sam}))$ are generated, each particle weight should be evaluated based on the measurement vector $\boldsymbol{P}(n)$. The weighted particles represent the posterior

probability density function of $p(R(n)\,|\boldsymbol{P}(1:n))$. For the particle weight evaluation, we propose several likelihood functions. The likelihood functions should be chosen to reflect the fact that the respiratory rate is chosen as the pole angle with the highest pole magnitude. They should also reflect the fact that the pole angle with the highest pole magnitude is occasionally an incorrect respiratory rate especially with a low SNR, as shown in our simulation example. In this study, we examined five different likelihood functions: the strongest neighbor (SN) likelihood, the nearest neighbor (NN) likelihood, the weighted nearest neighbor (WNN) likelihood, the probability data association (PDA) likelihood, and the weighted probability data association (WPDA) likelihood.

1) SN Likelihood: The idea of the SN likelihood we have developed is based on SN filtering [24], [25]. In SN filtering, the measurement with the highest intensity among the validated measurements is used and the others are discarded. Using the same concept, each particle weight is evaluated by the pole angle with the highest pole magnitude as

$$w^i(n) = L_{\mathrm{SN}}(p^a_{\max}\,|R^i\ (n)) = \exp\left(-\frac{\left(R^i(n)-p^a_{\max}\right)^2}{2\sigma^2_{\mathrm{gau}}}\right) \tag{11}$$

where $L_{\mathrm{SN}}(\cdot)$ is the SN likelihood operator for a particle weight evaluation, $i=\{1,2,\ldots I\}$, and $p^a_{\max}$ is the pole angle with the highest pole magnitude among the K_{roi} pole angles.

2) NN and WNN Likelihood: The idea of the NN likelihood we have developed is based on NN filtering [25], [26]. In NN filtering, the measurement closest to the predicted one is used, and the others are discarded. With the same concept, each particle weight is evaluated by its own nearest pole angle as

$$w^i(n) = L_{\mathrm{NN}}(p^a_{\mathrm{nn}(i)}\,|R^i\ (n)) = \exp\left(-\frac{\left(R^i(n)-p^a_{\mathrm{nn}(i)}\right)^2}{2\sigma^2_{\mathrm{gau}}}\right) \tag{12-1}$$

where $L_{\mathrm{NN}}(\cdot)$ is the NN likelihood operator for a particle weight evaluation, $i=\{1,2,\ldots I\}$, and $p^a_{\mathrm{nn}(i)}$ is the pole angle closest to each particle of $R^i(n)$.

The WNN likelihood extends the NN likelihood concept by weighting each pole angle's magnitude as

$$w^i(n) = L_{\mathrm{WNN}}\left(p^a_{\mathrm{nn}(i)}\,|R^i\ (n)\right) = \exp\left(-\frac{\left(R^i(n)-p^a_{\mathrm{nn}(i)}\right)^2}{2\sigma^2_{\mathrm{gau}}}\right)\frac{\exp\left(-\frac{\left(p^m_{\mathrm{nn}(i)}-p^a_{\max}\right)^2}{2\sigma^2_w}\right)}{\sum_{m=1}^{K_{\mathrm{roi}}}\exp\left(-\frac{\left(p^m_{\mathrm{nn}(i)}-p^a_{\max}\right)^2}{2\sigma^2_w}\right)} \tag{12-2}$$

where $L_{\mathrm{WNN}}(\cdot)$ is the WNN likelihood operator for a particle weight evaluation, $i=\{1,2,\ldots I\}$, and $p^m_{\mathrm{nn}(i)}$ is the pole magnitude corresponding to the pole angle $p^a_{\mathrm{nn}(i)}$.

3) PDA and WPDA Likelihood: The idea of the PDA likelihood we have developed is based on PDA filtering [25], [27]. The PDA uses all of the data with different weights. For example, each particle weight is evaluated by all pole angles instead of using only one pole angle, defined as

$$w^{i,k}(n) = L_{\mathrm{PDA}}\left(\boldsymbol{P}(n)\,|R^i\ (n)\right) = \exp\left(-\frac{\left(R^i(n)-p^a_k\right)^2}{2\sigma^2_{\mathrm{gau}}}\right) \tag{13-1}$$

where $L_{\mathrm{PDA}}(\cdot)$ is the PDA likelihood operator for particle weight evaluation, $i=\{1,2,\ldots I\}$, $k=\{1,2,\ldots K_{\mathrm{roi}}\}$. Based on this configuration $I\times K_{\mathrm{roi}}$ particle weights are evaluated. Note that each particle has multiple weights from which we can obtain multiple posterior probability density functions. Accordingly, we denote these particles by $R^{i,k}(n)$, where $i=\{1,2,\ldots I\}$ and $k=\{1,2,\ldots K_{\mathrm{roi}}\}$.

Similar to WNN likelihood, the WPDA likelihood function extends the PDA likelihood concept by weighting each pole angle's magnitude as the following:

$$w^{i,k}(n) = L_{\mathrm{WPDA}}\left(\mathbf{P}(n)\,|R^i\ (n)\right) = \exp\left(-\frac{\left(R^i(n)-p^a_k\right)^2}{2\sigma^2_{\mathrm{gau}}}\right) \times \frac{\exp\left(-(p^m_k-p^a_{\max})^2\Big/2\sigma^2_w\right)}{\sum_{m=1}^{K_{\mathrm{roi}}}\exp\left(-(p^m_k-p^a_{\max})^2\Big/2\sigma^2_w\right)} \tag{13-2}$$

where $L_{\mathrm{WPDA}}(\cdot)$ is the WPDA likelihood operator for a particle weight evaluation, $i=\{1,2,\ldots I\}$ and $k=\{1,2,\ldots K_{\mathrm{res}}\}$.

4) Weight Normalization and Resampling: For respiratory rate calculation, we normalize the particle weights as

$$\bar{w}^i(n) = \frac{w^i(n)}{\sum_{i=1}^{I} w^i(n)} \qquad \text{for SN, NN, and WNN} \tag{14-1}$$

and

$$\bar{w}^{i,k}(n) = \frac{w^{i,k}(n)}{\sum_{k=1}^{K}\left(\sum_{i=1}^{I} w^{i,k}(n)\right)} \qquad \text{for PDA and WPDA.} \tag{14-2}$$

After particle weight normalization, we calculate the mean of the particles' posterior probability density for the respiratory rate extraction. Once the mean of the particles' posterior probability density has been calculated, we resample the particles to generate new particles at the next time instant, $n+n_{\mathrm{sam}}$. The basic idea of resampling is to eliminate particles that have small weights and to concentrate on particles with large weights. In addition, the resampling process reduces the degeneracy problem, where after a few iterations, all but one particle will have negligible weight [16], [28]. As noted in the previous section, the resampled particles are denoted by $\overline{R}^i(n)$. Once the particles have been normalized, the resampled particles are generated using the scheme depicted in Fig. 3. In Fig. 3(a), the *I* to *I* resampling process is illustrated for the SN-, NN-, and WNN likelihoods. In Fig. 3(b), the $I\times K_{\mathrm{roi}}$ to *I* resampling process is illustrated for the PDA- and WPDA likelihoods.

E. PPG Data Collection on Human Subjects

1) Simulation Procedures: To evaluate the proposed PF algorithms for respiratory rate estimation, simulations using the test signal as described in (3) were performed with additive

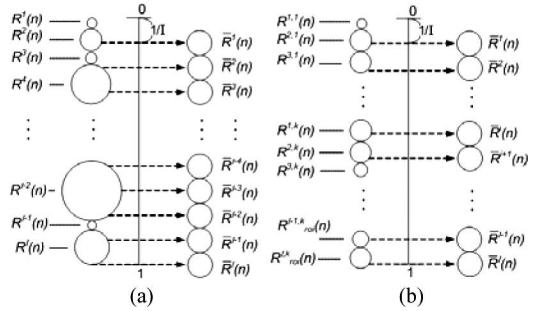

Fig. 3. Illustration of resampling processes: (a) *I* to *I* resampling for SN-, NN-, and WNN likelihoods, (b) $I \times K_{\mathrm{roi}}$ to *I* resampling for PDA- and WPDA likelihoods. The sizes of the circles represent the value of each particle weight.

GWN (AGWN) so that the SNR was -20 dB. The respiratory rate estimation performance was compared among six methods: SN-PF, NN-PF, WNN-PF, PDA-PF, WPDA-PF, and OPS only. We used 100 particles for all realizations including comparison to both experimental and simulated data. For an initial set of particles, the pole angle with the highest magnitude in the beginning of the time sample was chosen. For quantitative comparison of all methods, a root mean square error (RMSE) *E(n)* between $\widehat{R}(n)$ and $R(n)$ was computed, where $\widehat{R}(n)$ and $R(n)$ represent an estimated and a true respiratory rate of the waveform segment at time *n*, respectively. For every realization, 55 $\widehat{R}(n)$ were estimated (i.e., $n = \{60, 70, \ldots, 600\}$). In addition, we defined a deviation percentage. The deviation percentage denotes how many of the estimated respiratory rates deviate more than Th_{dev} from a true rate. We counted the deviation as

$$\left|\widehat{R}(n) - R(n)\right| > Th_{\mathrm{dev}}. \tag{15}$$

In the simulation result, we set Th_{dev} to 0.2, 0.3, and 0.4 Hz. In addition, we set the initial model order for the OPS to 30. The breathing rate of interest was set to $f_{\mathrm{low}} = 0.15$ Hz and $f_{\mathrm{high}} = 0.9$ Hz. An important issue in PF design is the choice of the variance of the particle sampling density (particle distribution) [29]. Thus, the values of σ^2_{gen}, σ^2_{gau}, and σ^2_w play important roles in determining estimation accuracy. The value of σ^2_{gen} represents the variance of generated particles as described in (9), and the chosen value predefines the range of the predicted respiratory rate. A selected value of σ^2_{gen} should not deviate too much from the selected chosen pole magnitude via the OPS. The values of σ^2_{gau} and σ^2_w represent the variances of likelihood functions as described in (11)–(13). Specifically, a choice of σ^2_{gau} determines the spread of pole angles each particle weight is evaluated, and likewise for the choice of σ^2_w for the likelihood functions of WNN-PF and WPDA-PF. For NN-PF and PDA-PF, we set $\sigma^2_w = \infty$ in (12-2) and (13-2), which results in (12-1) and (13-1), respectively. For other likelihood functions, the PF parameters were set to $\sigma^2_{\mathrm{gen}} = 0.01$, $\sigma^2_{\mathrm{gau}} = 0.0001$, and $\sigma^2_w = 0.0025$.

2) PPG Data Collection on Human Subjects: For the PPG waveform acquisition, we used an MP506 pulse oximeter (Nellcor Oximax, Boulder, CO) reusable sensor (Durasensor DS-100 A), which incorporates a conditioning circuit and has an analog output of 4.864 kHz. The PPG waveforms were collected on 15 healthy subjects with metronome respiratory rates ranging from 0.2 to 0.6 Hz at an increment of 0.1 Hz, and eight additional healthy subjects instructed to breathe at the rates of 0.7 and 0.8 Hz. Finally, we recruited ten additional healthy subjects and they were instructed to breathe at the rates of 1.0, 1.2, and 1.5 Hz. We categorized the respiratory rates of 0.2 and 0.3 Hz as the LF, the rates of 0.4–0.6 Hz as the high frequency (HF), the rates of 0.7 and 0.8 Hz as the ultra-HF (UHF), and the rates of 1.0–1.5 Hz as the extremely HF (EHF). Among the 15 healthy subjects, seven females and eight males of age 21.0 ± 1.2 years were involved, in the eight healthy subjects (for UHF experiment), one female and seven males of age 28.4 ± 3.6 years participated, and in the ten healthy subjects (for EHF experiment), three females and seven males of age 26.7 ± 4.6 years participated. None of the subjects had cardiorespiratory or related pathologies.

The PPG data were collected in the supine and upright positions for subjects instructed to breathe in the LF, HF, and UHF ranges. For subjects in the EHF protocol, the PPG data were collected only in the upright position because many participants had trouble breathing at these high rates in the supine position. The pulse oximeter sensor was attached to the subjects' left index or middle finger. The subjects were instructed to breathe at a constant rate according to a timed beeping sound so that the subjects inhaled and exhaled when the beeping sound was heard. Three minutes of PPG data were collected for each position for the breathing rates consisting of LF, HF, and UHF. For EHF rates, only 1–2 min of PPG signals were collected because most subjects could not keep up with extremely high breathing rates. We also simultaneously measured respiration signals using the respitrace system, which uses inductive plethysmography to provide calibrated voltage outputs corresponding to rib cage and abdominal compartment volume changes. From the respitrace system, true respiratory rates were evaluated by counting the number of peaks in a given minute. For those subjects breathing at the EHF rates, we also measured their ECG signals.

For all signals, consisting of PPG, respiration, and ECG signals, we used the PowerLab/4sp (ADInstrument, Inc.) for data acquisition. The PowerLab/4sp was connected to a laptop via universal serial bus, and the Chart v4.2.2 software was used to sample the analog signal at 400 Hz for EHF data and 200 Hz for LF, HF, and UHF data. All PPG data were low-pass filtered to 10 Hz. We performed the respiratory rate estimation on 60 s segments for the LF, HF, and UHF data, while 30-s segment data were used for the EHF data. All data segments were shifted by 10 s for the entire PPG waveform recording. We set the initial model order to 30 for the OPS. The breathing rate of interest was set to $f_{\mathrm{low}} = 0.15$ Hz and $f_{\mathrm{high}} = 0.9$ Hz for LF, HF, and UHF data. For the EHF data, we set the breathing rate of interest to $f_{\mathrm{low}} = 0.15$ Hz and $f_b < f_{\mathrm{high}} < f_h$. Furthermore, in order to investigate the effect on the heart signal (f_h), we set an additional ROI as $f_{\mathrm{low}} = 0.15$ Hz and $f_b < f_{h.} < f_{\mathrm{high}}$. The PF parameters were set to $\sigma^2_{\mathrm{gen}} = 0.01$, $\sigma^2_{\mathrm{gau}} = 0.0001$, and $\sigma^2_w = 0.0025$, which are the same as in the simulation example.

III. Results

A. Simulation Results

Fig. 4 shows the results of respiratory rate estimation by the OPS only (without the PF) and five different PF methods

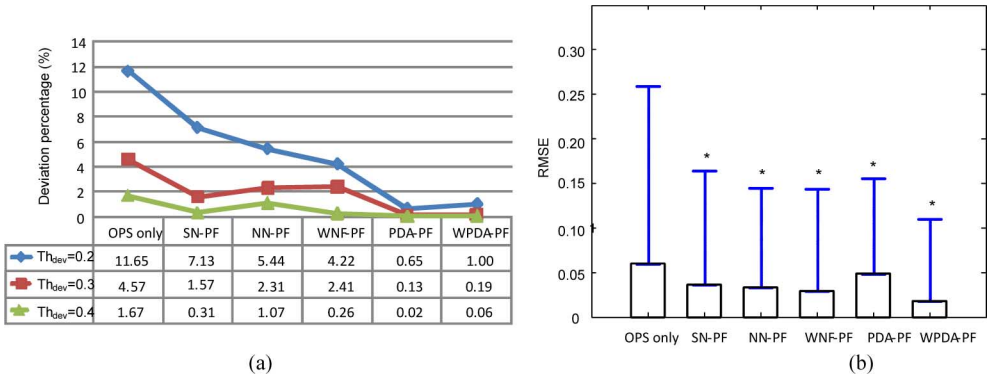

Fig. 4. One-hundred simulations were performed so that the respiratory rate was estimated a total of 5500 times, and the number of particles used was 100. (a) Deviation percentages were calculated as the total number of deviation divided by 5500 and multiplied by 100. Each deviation percentage is shown according to Th_{dev} from 0.2, 0.3, and 0.4 and each PF algorithm, (b) mean of RMSE and mean plus two standard deviations with the 5500 samples is shown, and the asterisks indicate the significant difference ($p < 0.01$) between OPS only and each PF algorithm.

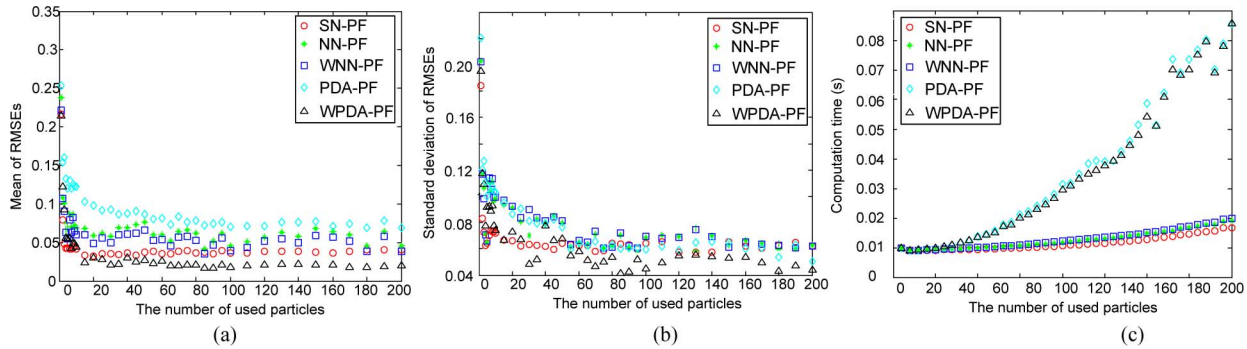

Fig. 5. Mean, standard deviation, and computation time of the average of 100 realizations according to the number of particles used from 1 to 200. (a) Mean of RMSEs. (b) Standard deviation of RMSEs. (c) Computational time (programs running on MATLAB R2007b).

consisting of SN-PF, NN-PF, WNN-PF, PDA-PF, and WPDA-PF with the test signal as described in (3). It summarizes the breathing frequency of 0.4 Hz based on 100 realizations for each method, which resulted in the estimation of 5500 respiratory rates. Fig. 4(a) shows the deviation percentages defined in (15). We report deviation percentage as a function of three different Th_{dev} values: 0.2, 0.3, and 0.4. Regardless of the chosen threshold value, both PDA-PF and WPDA-PF showed the smallest deviation percentage, while the OPS had the largest. Fig. 4(b) shows the mean of RMSE and its mean plus two standard deviations. All PF methods showed smaller RMSE values than OPS only. The asterisks indicate the significant difference ($p < 0.01$) between OPS only and each of the five different likelihood functions. Among the PF methods, there was no significant difference. Fig. 5(a)–(c) summarizes the mean and standard deviation of the RMSEs and the computation time as the number of particles varied from 1 to 200. These results suggest that approximately only 25 particles are needed to obtain reasonably accurate results for all proposed PF methods. There was a significant increase in the computation time with both PDA-PF and WPDA-PF when the number of particles was higher than 75.

B. Experimental Data Results

1) Result of LF, HF, and UHF Respiratory Rate: Figs. 6 and 7 show the RMSEs for each method for LF (0.2–0.3 Hz), HF (0.4–0.6 Hz), and UHF (0.7–0.8 Hz) during the supine and upright positions, respectively. The circles (red) above and below each method represent the 95th and the 5th percentiles of all estimation results for every subject, respectively. Whiskers (blue) above and below represent the 90th and the 10th percentiles, respectively. The bars above, middle, and below represent the 75th, the 50th, and the 25th percentiles, respectively. In addition, the asterisks indicate the mean value. Tables II and III summarize the measures of accuracy by tabulating the mean and variance of RMSE across all subjects for both supine and upright positions. For the statistical analysis, t-test ($p < 0.01$) was used among the six methods.

In the supine position, as shown in Fig. 6 and Table II, the mean of RMSE with WNN-PF was the lowest followed by NN-PF, WPDA-PF, PDA-PF, SN-PF, and OPS only for the LF respiratory rates. Similarly, the variances of RMSE with NN-PF, WNN-PF, and PDA-PF were the lowest followed by WPDA-PF, SN-PF, and OPS only. For the HF respiratory rates, the mean of RMSE with NN-PF was the lowest followed by WNN-PF, PDA-PF, WPDA-PF, SN-PF, and OPS only. The variance of RMSE with PDA-PF was the lowest followed by NN-PF, WNN-PF, WPDA-PF, SN-PF, and OPS only. For the UHF, the mean of RMSE with PDA-PF was the lowest followed by NN-PF, WNNA-PF, WPDA-PF, SN-PF, and OPS only. Similarly, the variance of RMSE with PDA-PF was the lowest followed by WPDA-PF, WNN-PF, NN-PF, SN-PF, and OPS only. Based

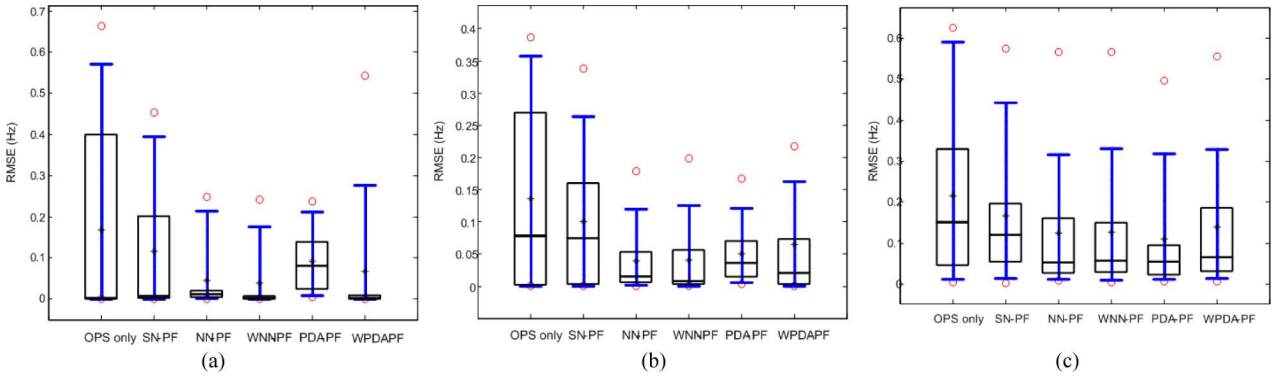

Fig. 6. RMSEs in the respiratory range of LF (0.2–0.3 Hz), HF (0.4–0.6), and UHF (0.7–0.8) for the supine position: (a) RMSEs for LF range (0.2–0.3 Hz), (b) RMSEs for HF range (0.4–0.6 Hz), (c) RMSEs for UHF range (0.7–0.8 Hz). The circles (red) above and below each method represent the 95th and the 5th percentiles of all estimation results for every subject with 16 segments, respectively. Whiskers (blue) above and below represent the 90th and the 10th percentiles, respectively. The bars above, middle, and below represent the 75th, the 50th, and the 25th percentiles, respectively. The asterisks indicate the mean value.

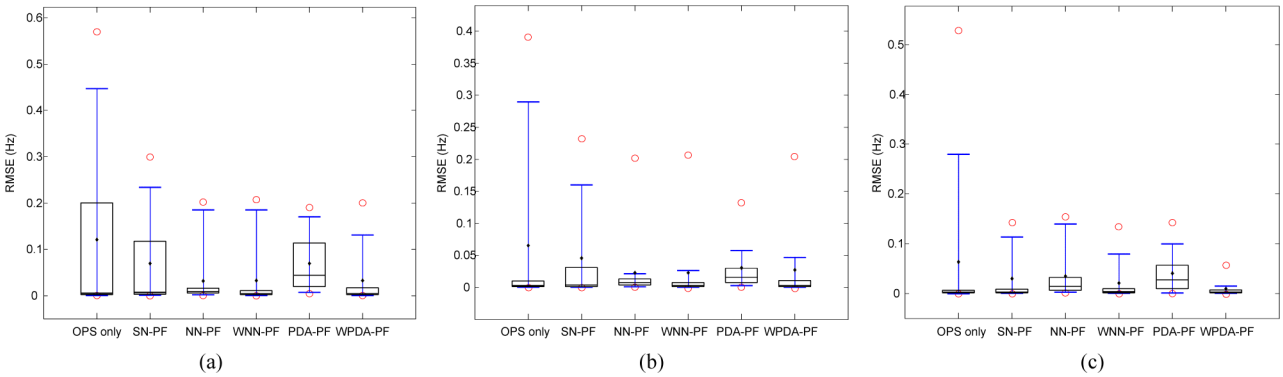

Fig. 7. RMSEs in the respiratory range of LF (0.2–0.3 Hz), HF (0.4–0.6), and UHF (0.7–0.8) for the upright position: (a) RMSEs for LF range (0.2–0.3 Hz), (b) RMSEs for HF range (0.4–0.6 Hz), (c) RMSEs for UHF range (0.7–0.8 Hz). The circles (red) above and below each method represent the 95th and the 5th percentiles of all estimation results for every subject with 16 segments, respectively. Whiskers (blue) above and below represent the 90th and the 10th percentiles, respectively. The bars above, middle, and below represent the 75th, the 50th, and the 25th percentiles, respectively. The asterisks indicate the mean value.

on the RMSE distribution, all five proposed PF methods showed significantly lower RMSEs than OPS only in both LF and HF respiratory rates. In the UHF respiratory rate range, the four PF methods NN-PF, WNN-PF, PDA-PF, and WPDA-PF all showed significantly lower RMSE than OPS only. Among the PF methods, in the LF respiratory rates, NN-PF, WNN-PF, and PDA-PF showed significantly lower RMSE than SN-PF. Also, NN-PF and WNN-PF showed significantly lower RMSE than WPDA-PF. There was no significant difference between NN-PF and WNN-PF. In the HF respiratory rates, NN-PF, WNN-PF, PDA-PF, and WPDA-PF showed significantly lower RMSE than SN-PF. There was no significant difference among the four methods. In the UHF respiratory rates, there was no significantly difference among the PF methods.

In the upright position, as shown in Fig. 7 and Table III, the means of RMSE with NN-PF, WNN-PF, and WPDA-PF were the lowest followed by PDA-PF, SN-PF, and OPS for the LF respiratory rates. The variance of RMSE with PDA-PF was the lowest followed by NN-PF, WPDA-PF, PDA-PF, SN-PF, and OPS. For the HF respiratory rates, the means of RMSE with NN-PF, WNN-PF, and WPDA-PF were the lowest followed by PDA-PF, SN-PF, and OPS. The variance of RMSE with PDA-PF was the lowest followed by NN-PF, WNN-PF, WPDA-PF, SN-PF, and OPS. For the UHF, the mean of RMSE with WPDA-PF was the lowest followed by WNN-PF, SN-PF, NN-PF, PDA-PF, and OPS. The variance of RMSE with PDA-PF was the lowest followed by WNN-PF, NN-PF, WPDA-PF, SN-PF, and OPS. Based on the RMSE distribution, all five proposed PF methods showed significantly lower RMSE than OPS only in all respiratory ranges of LF, HF, and UHF. In addition, among the PF methods, the same significant differences were observed in the supine position. Thus, regardless of subject positions, NN-PF and WNN-PF showed significantly lowest RMSE than any other method for the LF respiratory rate. For the HF respiratory rate, NN-PF, WNN-PF, PDA-PF, and WPDA-PF showed significantly lowest RMSE than any other method. For the UHF respiratory rate, all proposed methods showed significantly lowest RMSE. As shown in Fig. 5(c), PDA-PF and WPDA-PF requires much more computation time than NN-PF and WNN-PF, it is concluded that NN-PF and WNN-PF achieved the best result for LF, HF, and UHF respiratory rates.

2) Result of EHF Respiratory Rate: Fig. 8(a) shows the RMSE for each method for EHF (1.0–1.5 Hz) breathing rates during the upright position. For these EHF rates, the breathing frequency (f_b) may possibly overlap with a heart rate frequency (f_h), thus we set the range of interest from $f_{\text{low}} = 0.15$ Hz to

TABLE II
MEANS AND VARIANCES OF RMSES AND CORRESPONDING STATISTICAL SIGNIFICANCE WITH *P*-VALUES OF SIX METHODS IN RESPIRATORY RANGES LF (0.2–0.3 HZ), HF (0.4–0.6 HZ), AND UHF (0.7–0.8 HZ) FOR SUPINE POSITION: MEANS AND VARIANCES OF RMSES

Position	True Rate (Hz)	OPS only		SN-PF		NN-PF		WNN-PF		PDA-PF		WPDA-PF	
		Mean of RMSE (Hz)	Variance of RMSE (Hz)	Mean of RMSE (Hz)	Variance of RMSE (Hz)	Mean of RMSE (Hz)	Variance of RMSE (Hz)	Mean of RMSE (Hz)	Variance of RMSE (Hz)	Mean of RMSE (Hz)	Variance of RMSE (Hz)	Mean of RMSE (Hz)	Variance of RMSE (Hz)
Supine	LF (0.2 ~ 0.3)	0.1688	0.0593	0.1167	0.0270	0.0446	0.0061	0.0390	0.0063	0.0910	0.0061	0.0675	0.0248
	HF (0.4 ~ 0.6)	0.1356	0.0211	0.0997	0.0118	0.0394	0.0030	0.0450	0.0038	0.0512	0.0024	0.0646	0.0078
	UHF (0.7 ~ 0.8)	0.2160	0.0442	0.1666	0.0267	0.1257	0.0267	0.1278	0.0267	0.1104	0.0212	0.1386	0.0248

TABLE III
MEANS AND VARIANCES OF RMSES AND CORRESPONDING STATISTICAL SIGNIFICANCE WITH *P*-VALUES OF SIX METHODS IN RESPIRATORY RANGES LF (0.2–0.3 HZ), HF (0.4–0.6 HZ), AND UHF (0.7–0.8 HZ) FOR UPRIGHT POSITION: MEANS AND VARIANCES OF RMSES

Position	True Rate (Hz)	OPS only		SN-PF		NN-PF		WNN-PF		PDA-PF		WPDA-PF	
		Mean of RMSE (Hz)	Variance of RMSE (Hz)	Mean of RMSE (Hz)	Variance of RMSE (Hz)	Mean of RMSE (Hz)	Variance of RMSE (Hz)	Mean of RMSE (Hz)	Variance of RMSE (Hz)	Mean of RMSE (Hz)	Variance of RMSE (Hz)	Mean of RMSE (Hz)	Variance of RMSE (Hz)
Upright	LF (0.2 ~ 0.3)	0.1207	0.0371	0.0692	0.0113	0.0324	0.0040	0.0326	0.0052	0.0698	0.0037	0.0332	0.0043
	HF (0.4 ~ 0.6)	0.0654	0.0106	0.0461	0.0075	0.0232	0.0036	0.0230	0.0045	0.0305	0.0023	0.0273	0.0050
	UHF (0.7 ~ 0.8)	0.0633	0.0250	0.0301	0.0056	0.0348	0.0022	0.0214	0.0020	0.0413	0.0017	0.0103	0.0051

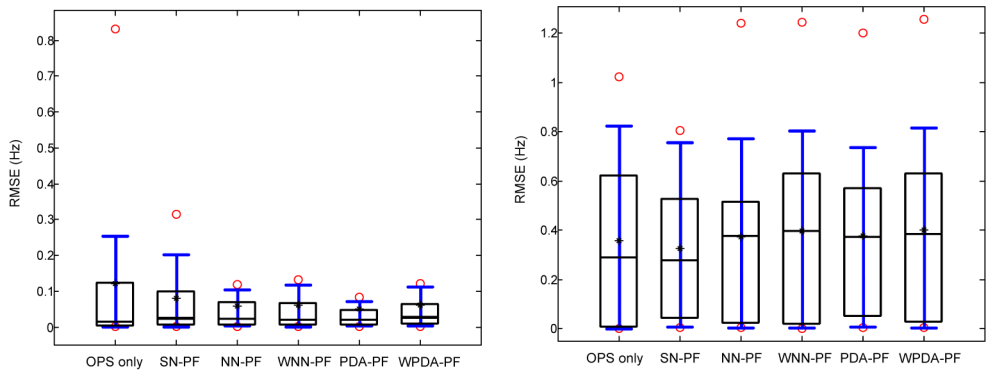

Fig. 8. RMSEs in the respiratory range of EHF (1.0–1.5 Hz) for the upright position: (a) RMSEs with $f_b < f_{\text{high}} < f_h$ (b) RMSEs with $f_b < f_h < f_{\text{high}}$. The circles (red) above and below each method represent the 95th and the 5th percentiles of all estimation results for every subject with 16 segments, respectively. Whiskers (blue) above and below represent the 90th and the 10th percentiles, respectively. The bars above, middle, and below represent the 75th, the 50th, and the 25th percentiles, respectively. The asterisks indicate the mean value.

$f_b < f_{\text{high}} < f_h$. For example, when the heart rate is 1.6 Hz and the respiratory rate is 1.2 Hz, f_{high} was set to 1.4 Hz. As shown in Fig. 8(a) and Table IV (first row), the mean value of RMSE with WNN-PF was the lowest followed by NN-PF, WPDA-PF, PDA-PF, SN-PF, and OPS. For the variance of RMSE values, PDA-PF, NN-PF, and WNN-PF were the lowest followed by WPDA-PF, SN-PF, and OPS. The proposed five likelihood functions showed significantly lower RMSE than OPS. Based on the RMSE distribution, all five proposed PF methods showed significantly lower RMSE than OPS only. Among the PF methods, there was no significant difference. Fig. 8(b) shows the RMSE for each method for EHF (1.0–1.5 Hz) when $f_b < f_h < f_{\text{high}}$ (the range of interest contains heart rate as well as respiratory rate). In this case, we observed that heart rate and respiratory rate were correctly detected approximately at only 60% and 40%, respectively, by the OPS technique. As shown in Fig. 8(b) and Table IV (second row), the respiratory rate extraction became inaccurate due to the heart rate detection. Consequently, there was no significant difference among all methods. Thus, for the respiratory rate extraction in the EHF range, we need to make sure that the heart and respiratory rates do not overlap. Otherwise, in most instances, the heart rate will be selected as the dominant pole instead of the respiratory frequency.

3) Discussion and Future Work: Spontaneous breath data result: We collected PPG data during spontaneous breathing from two male subjects. As a pilot demonstration of the robustness of our proposed method, we performed the respiratory rate estimation on 30 s segments for the entire 3 min data. The data segments were shifted by 10 s for the entire PPG recording, and the true respiratory rates were evaluated by counting the number of peaks measured from the respitrace system. For the OPS only, the mean and variance of RMSEs were 0.0347 and

TABLE IV
MEANS AND VARIANCES OF RMSES AND CORRESPONDING STATISTICAL SIGNIFICANCE WITH *P*-VALUES OF SIX METHODS IN RESPIRATORY RANGE OF EHF (1.0–1.5 HZ) FOR UPRIGHT POSITION: MEANS AND VARIANCES OF RMSES

	OPS only		SN-PF		NN-PF		WNN-PF		PDA-PF		WPDA-PF	
	Mean of RMSE (Hz)	Variance of RMSE (Hz)	Mean of RMSE (Hz)	Variance of RMSE (Hz)	Mean of RMSE (Hz)	Variance of RMSE (Hz)	Mean of RMSE (Hz)	Variance of RMSE (Hz)	Mean of RMSE (Hz)	Variance of RMSE (Hz)	Mean of RMSE (Hz)	Variance of RMSE (Hz)
$f_b<f_{high}<f_h$	0.1688	0.0593	0.1167	0.0270	0.04457	0.0061	0.0390	0.0063	0.0910	0.0061	0.0675	0.0248
$f_b<f_h<f_{high}$	0.1356	0.0211	0.0997	0.0118	0.0394	0.0030	0.0450	0.0038	0.0512	0.0024	0.0646	0.0078

0.0037, respectively, whereas they were 0.0149 and 0.0002 for WNN-PF.

Effect of initial set of particles: The performances of PF methods are affected by the initial set of particles chosen. In this paper, the initial set of particles was chosen based on the pole angle with the highest magnitude as determined by OPS. The accuracy of the PF method will certainly benefit and converge faster to a true solution if the initially chosen set of particles is closest to the true respiratory rate. This is the primary reason why we have combined the OPS with PF to obtain near-optimal solutions. For more accurate results than presented in this paper, a method, which provides the optimal initial set of particles, will need to be investigated.

Multiple dynamic model: In this study, we only considered fixing the breathing rate for the entire duration of the data recording. In the event of different breathing rates in a sample, the proposed method would not be optimal. For example, a subject might breathe at one rate and then either slowly or abruptly transition to a different breathing rate. To account for these different scenarios, a dynamic model is needed. For example, in the case of a constant breathing rate followed by an increase and then decrease in breathing rates, we may consider the following three models:

$$R^{i,j}(n) = F_j\left(\overline{R}^i(n-n_{\text{sam}})\right) + Q_2(n), \qquad \text{for } j = 1,2,3 \tag{16}$$

where

$$F_1\left(R(n-n_{\text{sam}})\right) = R(n-n_{\text{sam}}) \tag{17-1}$$

$$F_2\left(R(n-n_{\text{sam}})\right) = R(n-n_{\text{sam}}) + I_R \tag{17-2}$$

$$F_3\left(R(n-n_{\text{sam}})\right) = R(n-n_{\text{sam}}) - D_R \tag{17-3}$$

where I_R is the increased rate and D_R is the decreased rate. Note that $3 \times I$ predicted particles will be generated for these particular models. The question remains, however, how can we obtain the best values for the parameters I_R and D_R and dynamically change their weights depending on the breathing scenario since they are unknown. These questions will be investigated in our future work.

IV. CONCLUSION

We presented the combined OPS-PF algorithm and examined the robustness of five different likelihood functions for estimation of respiratory rates directly from pulse oximeter recordings. They were evaluated on 33 healthy subjects with a wide range of breathing rates varying from 0.2–1.5 Hz. We found that the combined OPS-PF approaches provided better accuracy than the solely OPS-based AR model for all breathing rates considered. The robustness of the combined OPS-PF approaches is evident as the accuracy is intact even for breathing rates as high as 1.5 Hz. This suggests that our proposed approach is also applicable for extracting breathing rates during exercise. We are not aware of any other algorithms that are able to provide such high breathing rates directly from a pulse oximeter. It should also be noted that the processing time was 10 ms for SN-PF, NN-PF, and WNN-PF, and 30 ms for PDA-PF and WPDA-PF. Thus the combined OPS-PF approach can be realizable in real time for practical applications.

REFERENCES

[1] K. H. Chon, S. Dash, and K. Ju, "Estimation of respiratory rate from photoplethysmogram data using time-frequency spectral estimation," *IEEE Trans. Biomed. Eng.*, vol. 56, no. 8, pp. 2054–2063, Aug. 2009.

[2] P. Leonard, T. F. Beattie, P. S. Addison, and J. N. Watson, "Standard pulse oximeters can be used to monitor respiratory rate," *Emerg. Med. J.*, vol. 20, no. 6, pp. 524–525, Nov. 2003.

[3] P. Leonard, T. D. Clifton, and P. S. Addison, J. N. Watson, and T. Beattie, "An automated algorithm for determining respiratory rate by photoplethysmogram in children," *Acta Paediatr.*, vol. 95, no. 9, pp. 1124–1128, Sep. 2006.

[4] P. Langley, E. Bowers, and A. Murray, "Principal component analysis as a tool for analysing beat-to-beat changes in electrocardiogram features: Application to electrocardiogram derived respiration," *IEEE Trans. Biomed. Eng.*, vol. 57, no. 4, pp. 821–829, Apr. 2009.

[5] P. S. Addison, "Secondary transform decoupling of shifted nonstationary signal modulation components: Application to photoplethysmography," *Int. J. Wavelets Multiresolution Inf. Process.*, vol. 2, no. 1, pp. 43–57, 2004.

[6] P. S. Addison, "Secondary wavelet feature decoupling (SWFD) and its use in detecting patient respiration from the photoplethysmogram," in *Proc. 25th Annu. Int. Conf. IEEE Eng. Med. Biol. Soc.*, 2003, vol. 3, no. 1, pp. 2602–2605.

[7] D. Clifton, J. G. Douglas, P. S. Addison, and J. Watson, "Measurement of respiratory rate from the photoplethysmogram in chest clinic patients," *J. Clin. Monit. Comput.*, vol. 21, no. 1, pp. 55–61, Feb. 2007.

[8] H. Wang, K. Siu, K. Ju, and K. H. Chon, "A high resolution approach to estimating time-frequency spectra and their amplitudes," *Ann. Biomed. Eng.*, vol. 34, no. 2, pp. 326–338, Feb. 2006.

[9] H. Wang, S. Lu, K. Ju, and K. H. Chon, "A new approach to closed-loop linear system identification via a vector autoregressive model," *Ann. Biomed. Eng.*, vol. 30, no. 9, pp. 1204–1214, 2002.

[10] R. Zou and K. H. Chon, "Robust algorithm for estimation of time-varying transfer functions," *IEEE Trans. Biomed. Eng.*, vol. 51, no. 2, pp. 219–228, Feb. 2004.

[11] J. Lee and K. H. Chon, "Respiratory rate extraction via an autoregressive model using the optimal parameter search criterion," *Ann. Biomed. Eng.*, DOI: 10.1007/s10439-010-0080-9, 2010.

[12] S. Lu, K. H. Ju, and K. H. Chon, "A new algorithm for linear and nonlinear ARMA model parameter estimation using affine geometry," *IEEE Trans. Biomed. Eng.*, vol. 48, no. 10, pp. 1116–1124, Oct. 2001.

[13] R. Zou, H. Wang, and K. H. Chon, "A robust time-varying identification algorithm using basis functions," *Ann. Biomed. Eng.*, vol. 31, no. 7, pp. 840–853, Jul.–Aug. 2003.

[14] L. Faes, G. Nollo, and K. H. Chon, "Assessment of Granger causality by nonlinear model identification: Application to short-term cardiovascular variability," *Ann. Biomed. Eng.*, vol. 36, no. 3, pp. 381–395, Mar. 2008.
[15] X. Xiao, Y. Li, and R. Mukkamala, "A model order selection criterion with applications to cardio-respiratory-renal systems," *IEEE Trans. Biomed. Eng.*, vol. 52, no. 3, pp. 445–453, Mar. 2005.
[16] M. S. Arulampalam, S. Maskell, N. Gordon, and T. Clapp, "A tutorial on particle filters for online nonlinear/non-Gaussian Bayesian tracking," *IEEE Trans. Signal Process.*, vol. 50, no. 2, pp. 174–188, Feb. 2002.
[17] J. H. Kotecha and P. M. Djuric, "Gaussian particle filtering," *IEEE Trans. Signal Process.*, vol. 51, no. 10, pp. 2592–2601, Oct. 2003.
[18] I. Smal, K. Draegestein, N. Galjart, W. Niessen, and E. Meijering, "Particle filtering for multiple object tracking in dynamic fluorescence microscopy images: Application to microtubule growth analysis," *IEEE Trans. Med. Imag.*, vol. 27, no. 6, pp. 789–804, Jun. 2008.
[19] Y. Rathi, N. Vaswani, and A. Tannenbaum, "A generic framework for tracking using particle filter with dynamic shape prior," *IEEE Trans. Image Process.*, vol. 16, no. 5, pp. 1370–1382, May 2007.
[20] A. C. Sankaranarayanan, A. Srivastava, and R. Chellappa, "Algorithmic and architectural optimizations for computationally efficient particle filtering," *IEEE Trans. Image Process.*, vol. 17, no. 5, pp. 737–748, May 2008.
[21] S. Hong, J. Lee, A. Athalye, P. M. Djuric, and W. D. Cho, "Design methodology for domain specific parameterizable particle filter realizations," *IEEE Trans. Circuits Syst. I*, vol. 54, no. 9, pp. 1987–2000, Sep. 2007.
[22] S. G. Fleming, "A comparison of signal processing techniques for the extraction of breathing rate from the photoplethysmogram," *Int. J. Biomed. Sci.*, vol. 2, no. 1, pp. 232–236, 2007.
[23] P. Leonard, N. R. Grubb, P. S. Addison *et al.*, "An algorithm for the detection of individual breaths from the pulse oximeter waveform," *J. Clin. Monit. Comput.*, vol. 18, no. 5–6, pp. 309–312, Dec. 2004.
[24] X. R. Li, "Tracking in clutter with strongest neighbor measurements-Part I: Theoretical analysis," *IEEE Trans. Autom. Control*, vol. 43, no. 11, pp. 1560–1578, Nov. 1998.
[25] Y. Bar-Shalom and W. D. Blair, *Multitarget-Multisensor Tracking: Applications and Advances*. vol. III, Norwood, MA: Artech House, 2000.
[26] A. Jadbabaie, J. Lin, and S. A. Morse, "Coordination of groups of mobile autonomous agents using nearest neighbor rules," *IEEE Trans. Autom. Control*, vol. 48, no. 6, pp. 988–1001, Jun. 2003.
[27] C. Rasmussen and G. D. Hager, "Probabilistic data association methods for tracking complex visual objects," *IEEE Trans. Pattern Anal. Mach. Intell.*, vol. 23, no. 6, pp. 560–576, Jun. 2001.
[28] M. Bolic, P. M. Djuric, and S. Hong, "Resampling algorithms and architectures for distributed particle filters," *IEEE Trans. Signal Process.*, vol. 53, no. 7, pp. 2442–2450, Jul. 2005.
[29] A. Doucet, S. Godsill, and C. Andrie, "On sequential Monte Carlo sampling methods for Bayesian filtering," *Stat. Comput.*, vol. 10, no. 3, pp. 197–208, Jul. 2000.

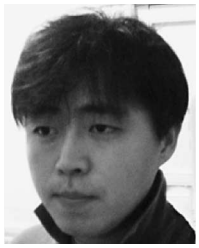

Jinseok Lee (M'09) received the dual B.S. degree in electrical engineering from both Stony Brook University, State University of New York, Stony Brook, NY, and Ajou University, Suwon, Korea, and the Ph.D. degree in electrical engineering from Stony Brook University.

He is currently a Postdoctoral Associate at the Department of Biomedical Engineering, Worcester Polytec hnic Institute, MA. His current research interests include medical instrumentation, low-power VLSI design for biomedical signal wireless communication, biomedical signal processing, and identification and modeling of physiological systems.

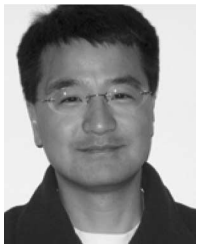

Ki H. Chon (SM'08) received the B.S. degree in electrical engineering from the University of Connecticut, Storrs, the M.S. degree in biomedical engineering from the University of Iowa, Iowa City, and the M.S. degree in electrical engineering and the Ph.D. degree in biomedical engineering from the University of Southern California, Los Angeles.

He is currently a Professor and the Chair at the Department of Biomedical Engineering, Worcester Polytechnic Institute, MA. His research interests include medical instrumentation, biomedical signal processing, and identification and modeling of physiological systems.

Prof. Chon is an Associate Editor of the IEEE TRANSACTIONS ON BIOMEDICAL ENGINEERING.